Available online at www.sciencedirect.com
SCIENCE DIRECT
Acta Materialia 54 (2006) 357–375
Acta MATERIALIA
www.actamat-journals.com

On modelling of dynamic recrystallisation of fcc materials with low stacking fault energy

C. Sommitsch [a,*], W. Mitter [b]

[a] Chair of Metal Forming, University of Leoben, Franz-Josef-Str. 18, A-8700 Leoben, Austria
[b] Institute of Mechanics, University of Leoben, Franz-Josef-Str. 18, A-8700 Leoben, Austria

Received 12 April 2005; received in revised form 11 August 2005; accepted 12 September 2005
Available online 24 October 2005

Abstract

A model for dynamic recrystallisation is presented, which was developed for face-centred cubic materials with low stacking fault energies. The critical conditions for nucleation are derived and a nucleation model is used that defines the nucleation rate as the velocity determining factor and that is based on the thermal climb of edge dislocations. Stable nuclei grow in dependence on the grain boundary mobility, thus a grain size distribution can be derived. During deformation, a time-dependent dislocation density gradient develops in the recrystallised grains, which leads to a corresponding dislocation density over all recrystallised grains. If the recrystallised grain fraction meets the critical conditions for the onset of recrystallisation, a second cycle will start. The development of grain size and recrystallised fraction is compared with measured data.

Keywords: Dynamic recrystallisation; EBSD; Hot working; Recovery

1. Introduction

During the hot forming of materials, strengthening and softening processes occur that lead to a certain microstructure and corresponding mechanical properties. Industrial processes such as rolling or forging try to fulfil the specifications of customers by an optimised thermo-mechanical processing and in addition make process simulation possible, on-line or off-line [1–3]. Simple Avrami-type models for the description of the grain structure development as a function of recrystallisation and grain growth have been established, whereby the necessary local strains and temperatures are supplied by finite element or finite difference models [4–6]. In addition ferritic steels show a matrix transformation which depends on both the austenite grain size and the cooling conditions [7]. A coupling between deformation and grain structure computation can be achieved, as the yield stress is derived from the actual structure conditions (i.e., grain size and effective strain).

A more physical description of the structure development on the mesoscopic–macroscopic level is reached, as one describes the temporal change of the dislocation density, and thus models recovery and recrystallisation [8–10]. For the latter process, an adequzate nucleation criterion must also be found with appropriate critical conditions. Additionally, in the case of precipitation and/or dissolution of particles, their effects on the yield stress have to be considered as well as the reciprocal effect between particle kinetics and recrystallisation and/or grain growth [11].

The model presented here deduces the dislocation density and the grain size distribution for the recrystallised and the deformed grains of a first and second recrystallisation cycle during hot forming. Meta-dynamic and static aspects will be discussed in a further publication. A one parameter model was selected that considers a mean dislocation density that is compared with a critical dislocation density for the onset of dynamic recrystallisation (DRX). Emphasis was put on the description of DRX, therefore

* Corresponding author. Tel.: +4338424025605; fax: +4338424025602.
E-mail address: christof.sommitsch@mu-leoben.at (C. Sommitsch).

1359-6454/$30.00
doi:10.1016/j.actamat.2005.09.008

the deformed state of matter was not modelled in detail. Hence, the following assumptions should only be valid for metals, where recrystallisation acts as the predominant softening mechanism. That should be sufficiently the case for nickel base alloys, austenitic steels and copper with their medium to low stacking fault energy [12,13], thus an exact modelling of dynamic recovery is not compellingly necessary hereby. Otherwise the evolution equations for the dislocation densities in the cell walls and inside the cell [14], both for the deformed unrecrystallised and the recrystallising grains, would have to be considered additionally. For the model validation, a comprehensive experimental program has been conducted for the nickel-base Alloy 80A [15,16].

The model here finds practical use in the optimisation of hot forming of nickel base superalloys and is in off-line use at Böhler Edelstahl GmbH, Austria. In order to ensure the demanded mechanical properties from rolled and forged products, a homogeneous and completely recrystallised structure must be achieved. The corresponding processing can substantially be improved by the numerical simulation of the structure development, coupled with finite elements analysis (FEA), in particular with regard to relatively small forming windows as well as to large gradients of temperature and deformation rate in large sized blooms. Contrary to semi-empirical models, the approach presented here can both consider recrystallisation cycles and the interaction of recrystallisation and precipitations [11]. Modelling of precipitation will not be considered explicitly in this work. In addition, the grain size distribution can be computed and the flow stress as a function of the mean dislocation density as an input parameter for the FEA is calculated. The model was tested for the nickel-base grades Alloy 80A as well as Alloy 718 for typical hot forming conditions for open die forging and radial forging ($950\,^{\circ}\mathrm{C} < T < 1200\,^{\circ}\mathrm{C}$, $0.01 < \dot{\varepsilon} < 10\ \mathrm{s}^{-1}$).

2. Experimental program

2.1. Compression tests

To confirm the simulation of DRX, experiments were performed on measured recrystallised fraction, nucleus density and grain size distribution [17]. Samples of Alloy 80A (Böhler L306 VMR, Table 1) were cut from hot rolled pieces, thus ensuring a completely recrystallised, fine-grained and homogeneous microstructure. Hot compression tests were carried out on a Gleeble 3800™ testing system in the temperature range ($950\,^{\circ}\mathrm{C} \leqslant T \leqslant 1200\,^{\circ}\mathrm{C}$) as well as the true strain rate domain ($0.01\ \mathrm{s}^{-1} \leqslant \dot{\varepsilon} \leqslant 10\ \mathrm{s}^{-1}$) relevant to the subsequently described model. Fig. 1(a) and (b) shows examples of stress–strain curves for temperatures of both 950 and 1150 °C and for different strain rates. Both the peak strain at maximum flow stress ε_p and the strain for steady-state stress ε_{ss} have been estimated by non-linear regression calculations

$$\varepsilon_p = 5.83 \times 10^{-4}\left[\dot{\varepsilon}\exp\left(\frac{582975}{R_g T}\right)\right]^{0.1081} \quad \text{for} \quad T \leqslant 1020\,^{\circ}\mathrm{C}, \tag{1a}$$

$$\varepsilon_p = 6.93 \times 10^{-2}\left[\dot{\varepsilon}\exp\left(\frac{476095}{R_g T}\right)\right]^{0.0244} \quad \text{for} \quad T > 1020\,^{\circ}\mathrm{C}, \tag{1b}$$

$$\varepsilon_{ss} = 0.360\left[\dot{\varepsilon}\exp\left(\frac{582975}{R_g T}\right)\right]^{0.0175} \quad \text{for} \quad T \leqslant 1020\,^{\circ}\mathrm{C}, \tag{2a}$$

$$\varepsilon_{ss} = 0.165\left[\dot{\varepsilon}\exp\left(\frac{476095}{R_g T}\right)\right]^{0.0342} \quad \text{for} \quad T > 1020\,^{\circ}\mathrm{C}. \tag{2b}$$

The separation in two temperature regimes is necessary in order to account for the precipitation of carbides and the γ'-phase $Ni_3(Al,Ti)$ in the lower temperature regime.

Prior to loading, a solution heat treatment was done at 1220 °C for 60 s. The short annealing time was chosen to avoid grain growth. This led to an initial grain size of 120 μm. A comprehensive microstructure analysis was performed at a test temperature of 1120 °C and at a constant strain rate of $0.1\ \mathrm{s}^{-1}$ at strains of 0.05, 0.10, …, 0.95, 1. This gives a peak strain of $\varepsilon_p = 0.178$ as well as the strain at steady-state flow stress of $\varepsilon_{ss} = 0.623$ according to Eqs. (1b) and (2b). The cylindrical compression samples ($h = 12$ mm, $d = 10$ mm) were cut to both longitudinal (specimen centre) and transversal cross-sections. The latter sections were carried out at a quarter of the specimen height. Finite element calculations of the compression tests proved that in this section from the centre to half the radius, the local and the global strain rate correspond. The investigations of the microstructure have been done both by an image analysis system and electron diffraction.

Table 1
Chemical composition of Alloy 80A (Böhler L306VMR) in weight per cent

C	Cr	Ti	Al	Ni
0.06	19.50	2.40	1.60	Bal.

2.2. Light microscopy (LIMI) and automatic image analysis

The ground and polished transversal and longitudinal sections were etched electrolytically. One quarter of every longitudinal and transversal section was evaluated by the commercial imaging system ImageC©. The first step in analysis was the transformation of the multi-colour image to a binary black and white image with closed grain boundaries (Fig. 2). Several standard tools of the imaging software were combined in a macro program to reach an optimum and reproducible transformation. Next a standard analysing tool of the software detected and calculated both the area and the chord length under 0°, 45°, 90° and 135° of every single grain. All grains overlapping with the image frame were excluded from

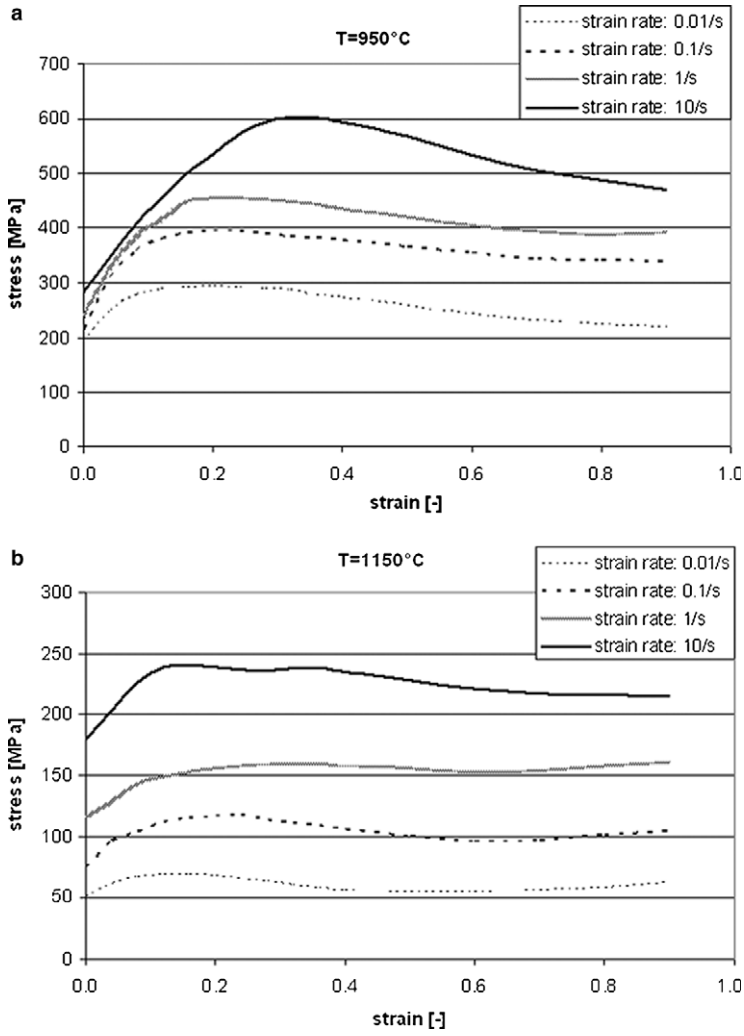

Fig. 1. Measured hot compression flow curves of Alloy 80A for different strain rates at $T = 950$ °C (a) and $T = 1150$ °C (b).

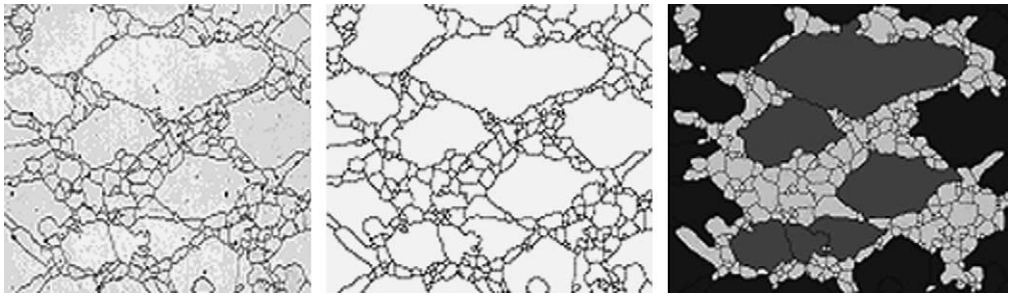

Fig. 2. DRX analysis by automatic image analysis of a sample of Alloy 80A at a local strain of $\varepsilon = 0.5$ [16]. Etched (a), binarised (b) and analysed (c) sections.

the evaluation. For the differentiation between the recrystallised grains and the deformed grains, both the diameter of the grain section area equal circle and the grain perimeter equal circle of an analysed grain were compared [17]. The quotient of these diameters was used as an indicator. This quotient is rather close to the ideal ratio (=1) of a circular area for the recrystallised grains. On the contrary, with increasing progress in the recrystallisation process the original grains develop a rather frayed boundary curvature. As a consequence their perimeter is strongly increasing. As an indicating parameter, the ratio of the diameter of a circle equivalent to the area to the diameter of a circle with the same length of the perimeter as that of the respective grain was used. A value of 0.125 was found to be an appropriate threshold.

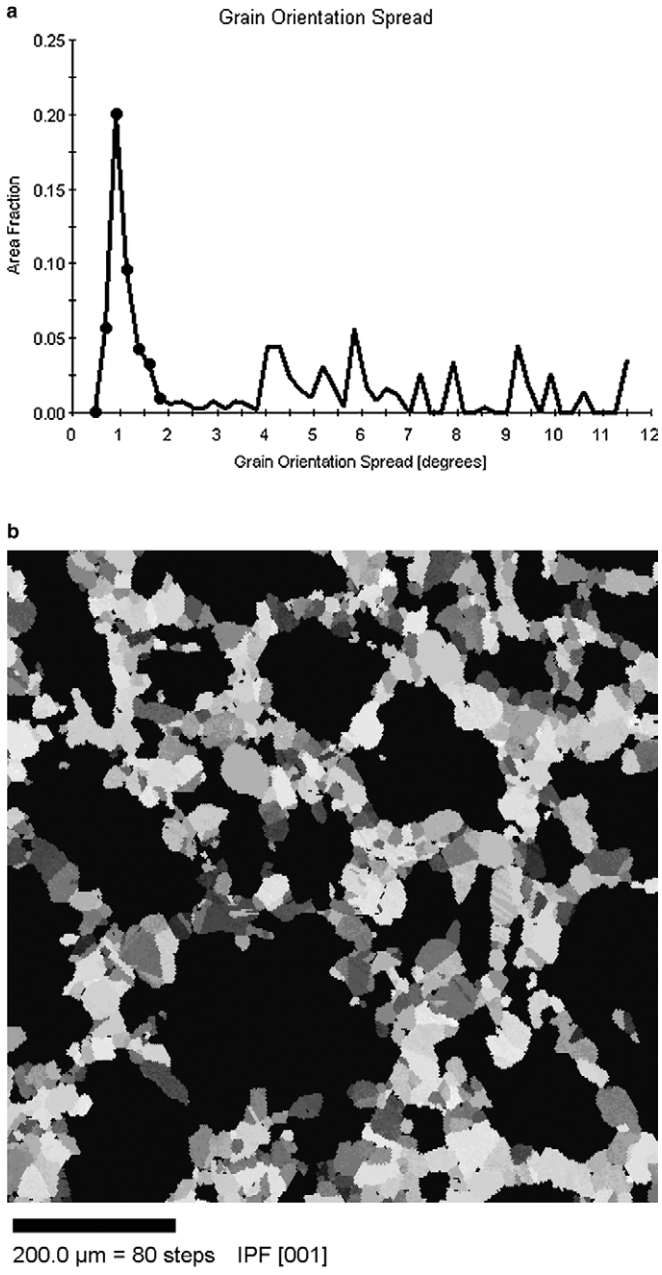

Fig. 3. (a) DRX analysis by EBSD of a sample of Alloy 80A at a local strain of $\varepsilon = 0.5$ [15]. In the orientation spread distribution of grains the maximal grain orientation spread of recrystallised grains is set to 2°. (b) The DRX grains show a necklace structure; deformed, not yet recrystallised grains in black.

2.3. Scanning electron microscopy (SEM) and electron backscatter diffraction (EBSD)

The investigations have been focused on the transversal cross-sections of the specimens [15]. The samples were polished using colloidal silica and analysed by a Leo Gemini 938™. The EBSD software OIM-TSL-Analysis 3© was used for the collection of orientation data as well as for the classification of grains due to their orientation difference (high angle grain boundary). The minimum orientation difference of two points of adjacent grains was fixed at 5°. Only grains with a minimum of six measuring points were considered which lead to an observable minimum grain size of 6 µm. Recrystallised and not yet recrystallised, i.e. deformed grains, were distinguished by the orientation spread within a grain (Fig. 3(a)). The area fractions of recrystallised and deformed grains were analysed in terms of grain size distributions, recrystallised fractions and DRX nucleus densities (Fig. 3(b)).

3. Criteria for the onset of dynamic recrystallisation

During hot forming, the time derivative of the dislocation density ρ_0 can be described [18] by the equation

$$\frac{\mathrm{d}\rho_0}{\mathrm{d}t} = \frac{\dot{\varepsilon}}{bl_0} - 2M\tau\rho_0^2, \tag{3a}$$

$$\rho_0(t) = \rho_s \tanh(2M\tau\rho_s t), \tag{3b}$$

taking the strain hardening and the recovery of dislocations into account but neglecting recrystallisation, where ρ_0 is the dislocation density of the unrecrystallised grains (denoted by the index 0), $\dot{\varepsilon}$ is the strain rate, b the Burgers vector, l_0 the mean free path of the dislocations ($l_0 \sim \rho_0^{-1/2}$), M the mobility of dislocations ($M \sim D_s b/k_B T$, [18]), D_s the self-diffusivity and τ the average energy per unit length of a dislocation. ρ_s is the steady-state value, which is obtained from Eq. (3a) setting $\mathrm{d}\rho_0/\mathrm{d}t = 0$. Eq. (3a) is a simplified form of a corresponding equation given by Stüwe [19,20]. In Eq. (3a), instead of l_0, also the mean radius r_{sub} of the subgrains of a cell structure can be chosen. From the work of Stüwe [19], it can be deduced that $r_{sub} \sim \rho_0^{-2/3} b^{-1/3}$. Instead of Eq. (3), similar approaches, e.g., those proposed by Kocks and Mecking [21] or Laasraoui and Jonas [22], could be used.

A critical dislocation density is necessary in order to initiate DRX and is related to the nucleation by the formation of a mobile high angle boundary under deformation conditions, which favour heterogeneity and hence dislocation accumulation. The nucleus usually forms at pre-existing grain boundaries in the material, at least at higher strain rates [13]. For low strain rates and large initial grain sizes, intra granular nucleation becomes relatively more important. Apart from the initial nucleation stage, the mean recrystallised grain size remains more or less constant during the recrystallisation, thus there is little or no simultaneous average grain growth (compare with Fig. 11).

Roberts and Ahlblom [23] developed a nucleation criterion, which is based upon the classical nucleation theory, applied to conditions of current deformation. During DRX, the concurrent deformation reduces the stored energy difference (i.e., driving force) that effects migration of a high angle boundary. Therefore, the driving force in the regions into which the reaction is proceeding must be higher for dynamic than for static recrystallisation if the boundary is to migrate at the same velocity. Fig. 4 schematically depicts the high angle boundary of a potential

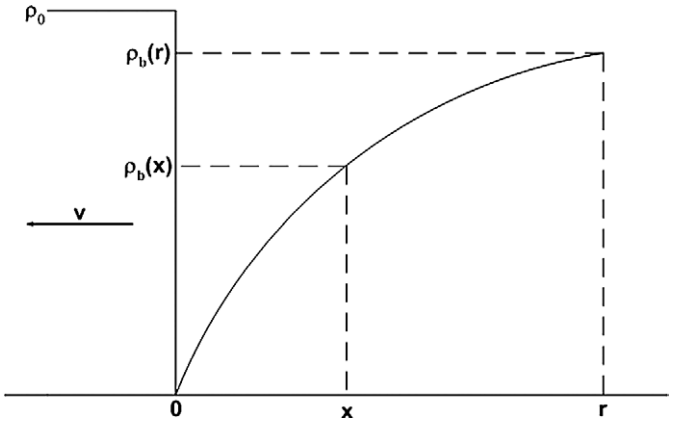

Fig. 4. Dislocation density development in the vicinity of a moving boundary of a recrystallising grain [23].

nucleus migrating from the right to left side with the velocity v.[1] For an area that has just been recrystallised it is assumed that the dislocation density ρ_0 generated by the preceding strain is reduced to a very low value. The nucleation theory gives the net free energy change [23]

$$\Delta G(r) = -\frac{4}{3}\pi r^3 \frac{\tau}{r}\int_0^r [\rho_0 - \rho_b(x)]\mathrm{d}x + 4\pi r^2 \gamma_{GB}, \tag{4}$$

where γ_{GB} is the grain boundary energy per unit area, $\rho_b(x)$ the increasing dislocation density behind the boundary (i.e., in the newly recrystallised grain) and r the radius of a spherical nucleus (Fig. 4). Maximising the net free energy change produces the critical nucleation conditions

$$r\tau\left[\frac{\rho_s}{3}\tanh\left(2\frac{M}{m}\frac{\rho_s}{\rho_0}r\right) - \rho_0\right] + \left(\frac{\tau\rho_0 m}{3M}\right)\ln\left[\cosh\left(2\frac{M}{m}\frac{\rho_s}{\rho_0}r\right)\right] + 2\gamma_{GB} = 0, \tag{5}$$

where m denotes the mobility of a moving high angle boundary and ρ_s the stationary dislocation density for dynamic recovery [23].[2] Eq. (5) is valid provided that ρ_0 stays constant, which is not really true (Eqs. (3a) and (3b)). However, ρ_0 remains within a rather small range between ρ_{cr} and ρ_s. Hence, this simplification is acceptable. In the model ρ_{cr} is the smallest ρ_0 as a function of r that is smaller than ρ_s. Eq. (5) is a transcendent highly non-linear equation in r and ρ_0. No real critical radius r_{cr} exists unless ρ_0 exceeds a critical value ρ_{cr}. Eq. (5) considers the case of intra granular nucleation. For the assumption of nucleation associated with the bulging mechanism, a critical dislocation density and a critical diameter were deduced [23]; these were about 12% higher and about 20% lower, respectively, than in the case of intra granular nucleation. These values have been used in order to modify the calculated r_{cr} and ρ_{cr} by Eq. (5).

In the following, an illuminating geometrical solution of the critical conditions for nucleation according to Eq. (5) will be accomplished. Therefore, the straight lines, defined by

$$2\frac{M}{m}\frac{\rho_s}{\rho_0}r = \xi \tag{6}$$

are intersected with the solution curve of Eq. (5) with the same parameter ξ. Fig. 5 shows an example of the intersection choosing a constant value of $\xi = 1$.

The intersection point in Fig. 5 meets the following equations:

$$r\tau\left[\frac{\rho_s}{3}\tanh(\xi) - \rho_0\right] + \left(\frac{\tau\rho_0 m}{3M}\right)\ln[\cosh(\xi)] + 2\gamma_{GB} = 0 \tag{7}$$

and

$$r = \frac{m\rho_0}{2M\rho_s}\xi. \tag{8}$$

For arbitrary ξ the respective intersection point in Fig. 5 represents a solution of Eq. (5). Substituting r from Eq. (8) into Eq. (7) leads to

$$\xi\frac{m\rho_0}{2M\rho_s}\tau\left[\frac{\rho_s}{3}\tanh(\xi) - \rho_0\right] + \left(\frac{\tau\rho_0 m}{3M}\right)\ln[\cosh(\xi)] + 2\gamma_{GB} = 0. \tag{9}$$

This is a quadratic equation for ρ_0 and can be solved explicitly with the assumption of $\rho_0 > 0$. A parametric representation of the solutions of Eq. (5) is given by

$$\rho_0(\xi) = \frac{\rho_s m\tau(\xi\tanh(\xi) + 2\ln(\cosh(\xi)))}{6m\tau\xi} + \frac{\sqrt{(\rho_s m\tau(\xi\tanh(\xi)) + 2\ln(\cosh(\xi)))^2 + 144\xi m\tau\gamma_{gb}M\rho_s}}{6m\tau\xi} \tag{10}$$

and inserting ρ_0 in Eq. (8) gives

$$r(\xi) = \frac{\rho_s m\tau(\xi\tanh(\xi) + 2\ln(\cosh(\xi)))}{12M\rho_s\tau} + \frac{\sqrt{(\rho_s m\tau(\xi\tanh(\xi)) + 2\ln(\cosh(\xi)))^2 + 144\xi m\tau\gamma_{gb}M\rho_s}}{12M\rho_s\tau}. \tag{11}$$

Fig. 5 shows a geometric solution of Eq. (5) for $\xi = 1$ as an example, where $\xi \in (0, \infty)$. For increasing ξ, lines G_ξ become flatter and approach the horizontal axis

$$\lim_{\xi\to\infty} r(\xi) = \infty, \quad \lim_{\xi\to\infty}\rho_0(\xi) = \rho_s \tag{12}$$

and for decreasing ξ, lines G_ξ become steeper and approach the vertical axis

[1] $x = r$ is the instantaneous coordinate of the nucleation site. At $x = 0$ the grain boundary is situated, where the point of origin is fixed. Therefore, the nucleation site is moving from left to right relative to this coordinate system.

[2] For making possible analytical integration, Roberts and Ahlblom [23] partly used plane instead of spherical geometry; see e.g., the averaging procedure according to Eq. (4). This does not involve notable reduction of precision.

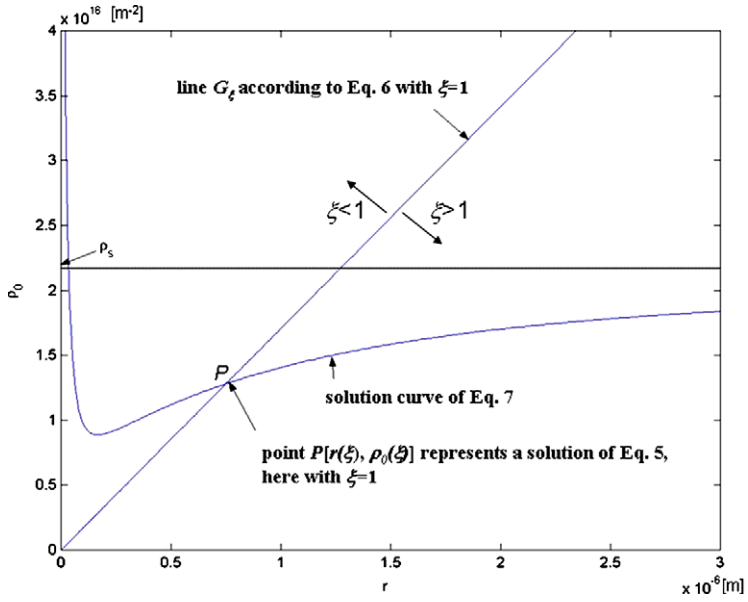

Fig. 5. Graphical depiction of the solution procedure. Intersection of the solution curve of Eq. (7) with line G_ξ for arbitrary $\xi = 1$. Example with adequately chosen hot forming parameters.

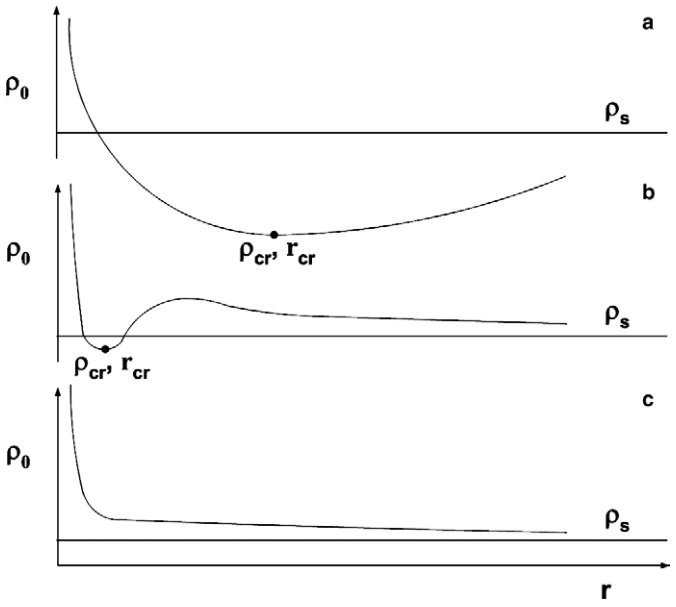

Fig. 6. Determination of the critical radius of a DRX nucleus and of the corresponding critical dislocation density for the onset of DRX according to Eq. (7) with variable radius r (schematic diagram). The critical dislocation density is found at the minimum of $\rho_0(r)$. Relatively low tendencies for dynamic recovery and a high grain boundary mobility promote a recrystallisation start (a); if the driving force for DRX depends (Eq. (4)) on the difference of ρ_s and ρ_{cr}, nucleation is only possible in a very narrow range and with a low tendency (b); if the local conditions are so that ρ_0 does not fall short of the stationary dislocation density ρ_s, no DRX will be initiated (c).

$$\lim_{\xi\to 0} r(\xi) = 0, \quad \lim_{\xi\to 0} \rho_0(\xi) = \infty. \tag{13}$$

For the calculation of ρ_{cr}, the function $\rho_0(\xi)$ from Eq. (10) has to be minimised. For the minimisation, the equation $\angle\rho_0(\xi)/\angle\xi = 0$ was solved by a modified Newton method

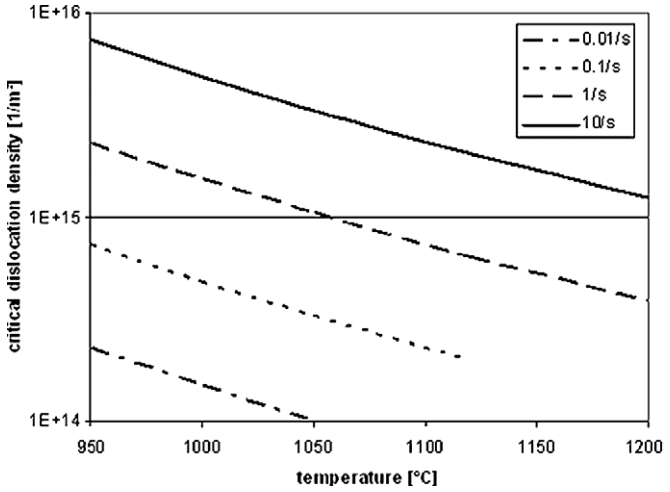

Fig. 7. Calculated critical dislocation density as a function of temperature and strain rate for Alloy 80A.

[24]. This gives the appropriate value of ξ as a function of the other parameters. Fig. 6 schematically shows three types of results that correspond to Eq. (5) and which depend on different deformation conditions. In Fig. 6(a), the conditions for DRX are favourable. With an increasing mobility of dislocations M (i.e., dynamic recovery) and with a decreasing mobility of high angle grain boundaries m (e.g., due to the precipitation of small particles) the conditions for the onset of recrystallisation get worse (Fig. 6(b)) or even impossible (Fig. 6(c)).

Obviously, DRX can only start if a critical dislocation density exists that falls short of the stationary dislocation density for dynamic recovery. Fig. 6(b) shows transition conditions where stable DRX nuclei can be formed but ρ_{cr} is only slightly lower than ρ_s. Hence with ongoing recrystallisation, the remaining driving force for grain boundary

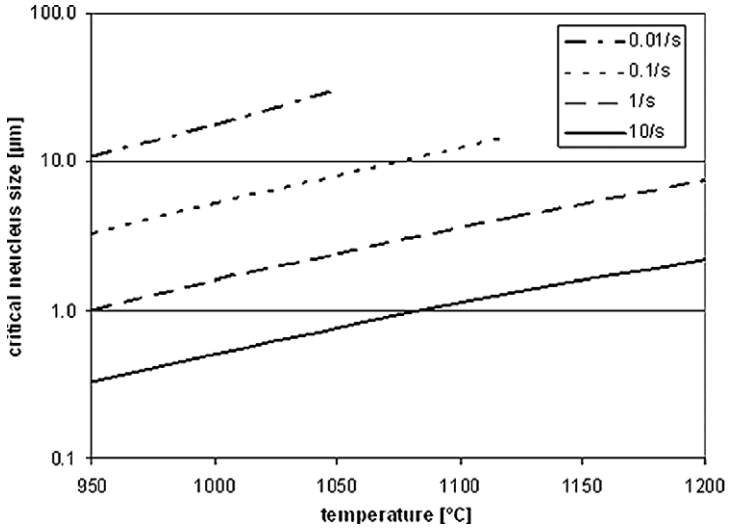

Fig. 8. Calculated critical nuclei size as a function of temperature and strain rate for Alloy 80A.

migration probably becomes sub-critical and recrystallisation will eventually stop. However, it is fairly questionable if the criterion used for recrystallisation, which does not consider the inhomogeneity of stored deformation energy, is able to describe incomplete recrystallisation.

Figs. 7 and 8 depict the development of the critical dislocation density and the critical nucleus size, respectively, in Alloy 80A in dependence on temperature and strain rate. Only those conditions are considered that meet the requirements of the onset of DRX, described above. Hence, no stable conditions have been found both for a strain rate of 0.01 s^{-1} or lower, above 1120 °C, and a strain rate of 0.1 s^{-1} or lower, above 1200 °C.

4. Nucleation rate

In the previous section, a model developed from Robert and Ahlblom [23] for the prediction of the critical dislocation density ρ_{cr}, as well as of the critical radius r_{cr} of a recrystallisation nucleus was stated. Hence, both the critical deformation ε_{cr} and the associated deformation time t_{cr} can be calculated with Eq. (3b). However, this nucleation condition, which is based on the classical nucleation theory, supplies no information about the mechanisms of nucleation and about the inhomogeneities that must be involved [23]. In order to get a mathematical expression for the nucleation rate, assumptions about nucleation and growth mechanisms as well as about the distribution of nucleation stimulating inhomogeneities are necessary, which are discussed in the following.

Dynamic discontinuous recrystallisation can be considered in terms of the rate of nucleation (formation of interfaces) versus the rate of growth (migration of interfaces) under given boundary conditions [25]. A model that considers the dynamic balance of these two rates was proposed by Srinivasan and Prasad [12]. The nucleation consists of the formation of a grain boundary due to dislocation generation and simultaneous recovery and rearrangement. This interface will become a nucleus for dynamic recrystallisation if it attains a critical size and configuration, i.e. a high angle grain boundary. The nucleus will grow by the process of grain boundary migration. Since under hot working conditions the material acts essentially as a dissipator of power, the driving force for the migration of interfaces is the reduction of total interface energy. If nucleation and growth occur simultaneously, the slower of the two will control DRX.

After reaching the critical dislocation density ρ_{cr} and the critical deformation ε_{cr}, respectively, new nuclei form with ongoing deformation. Let the probability for nucleation in case of $\varepsilon > \varepsilon_{cr}$ and within the range of ε and $\varepsilon + d\varepsilon$ be $P_N(\varepsilon, \dot{\varepsilon})\, d\varepsilon$ with

$$\int_{\varepsilon_{cr}}^{\infty} P_N(\varepsilon, \dot{\varepsilon})\, d\varepsilon = 1. \tag{14}$$

During a recrystallisation cycle, the number of nuclei that are formed between ε and $\varepsilon + d\varepsilon$ is dN

$$dN = N_P(t) P_N(\varepsilon, \dot{\varepsilon})\, d\varepsilon \tag{15}$$

and because of $d\varepsilon = \dot{\varepsilon}\, dt$ the nucleation rate per unit volume is given by

$$R_N(t) = \frac{dN}{dt} = N_P(t) P_N(\varepsilon, \dot{\varepsilon}) \dot{\varepsilon}. \tag{16}$$

Herein, $N_P(t)$ means the number of potential nuclei per volume, which equals the number of nucleation-stimulating inhomogeneities per volume, for which up to the time t no nuclei had yet formed. From Eq. (16) it is evident that $R_N(t)$ is proportional to $\dot{\varepsilon}$. For the determination of the function $[N_P(t) P_N(\varepsilon, \dot{\varepsilon})]$ the following considerations are employed. The rate of recovering groups of dislocations (interfaces) as a result of migration of interfaces depends upon the mobility of the boundary. On the other hand, the rate of interface formation is governed by the rate of generation of

recovered dislocations. In [12], it is shown that for nickel the rate of interface formation (nucleation) is lower than the rate of interface migration (growth) by about four orders of magnitude and therefore controls the dynamic recrystallisation process. For nickel, nickel-based superalloys, as well as austenitic steels with their relatively low stacking fault energies at high temperatures, mechanical recovery involving cross-slip of screw dislocations can be neglected in comparison with thermal recovery based on climb of edge dislocations. Therefore, the rate of generation of recovered dislocations R_F, i.e. the number of dislocations available for nucleation per unit area and unit time for these types of alloys, can be described by [12]

$$R_F = \frac{\dot{\varepsilon} P_R}{b l_0}. \tag{17}$$

In Eq. (17), $P_R = \exp(-Q_{SD}/RT)$ is the probability of recovery of dislocations, where Q_{SD} denotes the activation energy of self-diffusion that equals the activation energy for dislocation climb. The assumption above can be stated if $\rho_0 \geqslant \rho_{cr}$.

The origin of recrystallisation at pre-existing high angle grain boundaries is known to be a very important mechanism, especially at lower strains and at higher temperatures. Strain induced boundary migration may occur by the migration of a boundary due to different stored energies on both sides of the boundary. If we consider a poorly developed dislocation cell structure and large stored energy differences between the grains, it will occur by the migration of a boundary adjacent to several cells/subgrains [26]. In this model, nucleation is expected, if the bulged recovered area equals the size of an over-critical, i.e. stable nucleus.

If the initial grains are very large, e.g., what is expected for a primary as cast structure, the low specific grain boundary area can not act as the substantial nucleation stimulator, thus dynamic recovery and nucleation within the grains will become more relevant [27]. Nevertheless, if the critical conditions for the onset of recrystallisation are met, other nucleation mechanisms can become more important.

Let $N_d = A_{cr}/l_{cr}^2$ be the number of dislocations per critical nucleus, A_{cr} the cross-section of a critical nucleus and l_{cr} the mean free path of dislocations with a critical density ($l_{cr} \sim \rho^{-1/2}$), whereas N_d, A_{cr} as well as l_{cr} are time-dependent, if the deformation variables temperature and strain rate are changing with time. Therefore, R_F/N_d is the number of generated nuclei per unit area and unit time. If we assume that nuclei preferentially form at high angle grain boundaries of the deformed grains with mean diameter D_0, the grain boundary area per unit volume is proportional to the reciprocal of $D_0[D_0^2/D_0^3 = 1/D_0]$ and therefore $[R_F/(N_d D_0)]$ is proportional to the number of nuclei generated per unit volume and unit time. If K_F is a factor for accommodation to the experimental data, the nucleation rate per unit volume is

$$R_N(t) = \frac{K_F R_F(t)}{N_d(t) D_0} = \frac{K_F P_R}{b l_0 N_d(t) D_0} \dot{\varepsilon}. \tag{18}$$

A comparison with Eq. (16) gives

$$N_P(t) P_N(\varepsilon, \dot{\varepsilon}) = \frac{K_F P_R}{b l_0 N_d(t) D_0}. \tag{19}$$

Since the right side of Eq. (19) does not strongly depend on time t and thus on strain ε, the approximation in accordance with Eq. (18) is valid if the asymmetric bell curve $[N_P(t) P_N(\varepsilon, \dot{\varepsilon})]$ does not strongly change with ε and thus stays in the range of its plateau. That means that the growth of the recrystallised grains must be terminated, while the nucleation rate is still relatively high. As already mentioned above, this restriction applies to nickel and nickel-based alloys.

5. Recrystallisation rate

In the following, a new model is to be described that considers two recrystallisation cycles. These cycles are marked by the indices 1 and 2. The critical conditions for the onset of dynamic recrystallisation, as well as the nucleation rate, are input parameters for this model and thus can be predicted with the help of similar approaches.

The number of nuclei N per volume can be calculated at a time of observation t_b by

$$\begin{aligned} N_1(t_b) &= \int_{t_{cr1}}^{t_b} R_{N1}(t)(1 - f_1(t))\, dt \\ &= \int_{t_{cr1}}^{t_b} \frac{K_F R_{F1}(t)}{N_{d1}(t) D_0}(1 - f_1(t))\, dt \end{aligned} \tag{20}$$

with R_{F1} according to Eq. (17). In order to consider the decreasing area of potential nuclei formation with the ongoing recrystallisation, the nucleation rate is multiplied by $(1 - f_1)$, where f_1 is the recrystallised fraction of the first recrystallisation cycle. It is presupposed that the nucleation during the first recrystallisation cycle only proceeds in areas that are not recrystallised yet, since the recrystallised parts are strained sub-critical. Only during the following recrystallisation cycle can nuclei form within recrystallised grains of the first cycle. An expression for $f(t)$ is deduced below. For materials with high stacking fault energy and thus the affinity to form cell structure, a more precise model would have to think of nucleation in terms of recovery of sessile dislocations in the cell walls.

Fig. 9 depicts the calculated development of the nuclei density as a function of strain for Alloy 80A. Both the EBSD measurements and model data show slightly higher values than the LIMI results.

It is assumed that during recrystallisation for each time step Δt a grain class is formed, consisting of ΔN nuclei with the critical radius. At a time of observation t_b the size of a grain class corresponding to its time of generation $t_g > t_{cr1}$ can be determined by

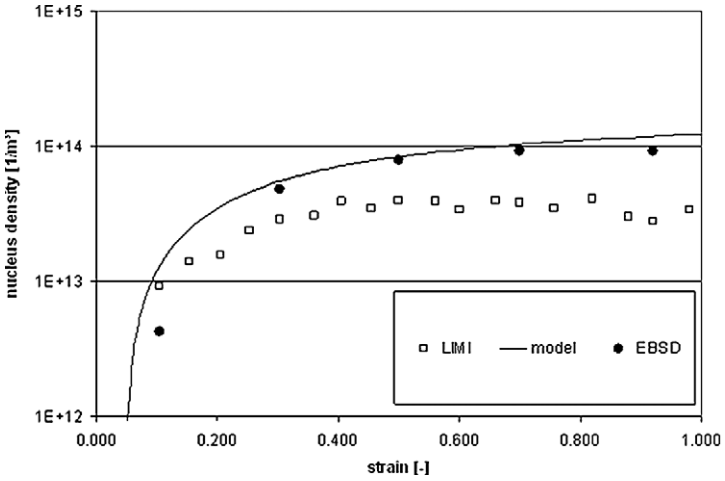

Fig. 9. Measured and calculated nuclei density at $T = 1120\ ^\circ\mathrm{C}$ and $\dot{\varepsilon} = 0.1\ \mathrm{s}^{-1}$ of Alloy 80A [17].

$$D_1(t_g, t_b) = D_{cr1}(t_g) + 2\int_{t_g}^{t_b} v_1(\tau)\,\mathrm{d}\tau, \tag{21}$$

with $D_{cr1} = 2r_{cr1}$ and t_g as the time of generation of a new grain class. The grain boundary velocity v_1 depends on time due to the precipitation of particles, changing temperature and strain rate. Hence, the velocity of a high angle boundary during recrystallisation is the product of the boundary mobility m, the sum of the driving and dragging forces and a diminishing factor K_S, therefore

$$v_1 = m(\tau\Delta\rho_1 - P_Z)K_S, \tag{22}$$

where P_Z is the Zener drag [28] and K_S is a factor that represents the solute drag for high boundary velocities [29]. $\tau\Delta\rho_1$ denotes the stored energy difference ($\Delta\rho_1 = \rho_0 - \rho_{b1}(x = 0) \approx \rho_0$) in the vicinity of the boundary, with ρ_0 as the mean dislocation density in the deformed grains and $\rho_{b1}(x = 0) \approx 0$, see Fig. 4.

Approximating the grains as spheres, the volume of one grain of this class is

$$V_1(t_g, t_b) = \frac{\pi}{6}D_1^3(t_g, t_b). \tag{23}$$

$[R_{N1}(t_g)(1 - f_1(t_g))\,\mathrm{d}t_g]$ grains are nucleated per unit volume in the time interval $[t_g, t_g + \mathrm{d}t_g]$. The volume of all grains which are nucleated per unit volume according to t_g and t_b within this time interval is $[V_1(t_g, t_b)R_{N1}(t_g)(1 - f_1(t_g))\,\mathrm{d}t_g]$. The recrystallised fraction $f_1(t_b)$ at the time t_b is given by the sum over all nucleation times, starting at the time t_{cr1}, where the dislocation density reaches the critical value ($\rho_0 \geqslant \rho_{cr1}$)

$$\begin{aligned} f_1(t_b) &= \int_{t_{cr1}}^{t_b} V_1(t_g, t_b)R_{N1}(t_g)(1 - f_1(t_g))\,\mathrm{d}t_g \\ &= \frac{\pi}{6}\int_{t_{cr1}}^{t_b} D_1^3(t_g, t_b)R_{N1}(t_g)(1 - f_1(t_g))\,\mathrm{d}t_g. \end{aligned} \tag{24}$$

The volume increase of a grain nucleated at the time t_g follows from Eqs. (21) and (23)

$$\begin{aligned} \mathrm{d}V_1(t_g, t_b) &= \frac{\mathrm{d}V_1(t_g, t_b)}{\mathrm{d}D_1(t_g, t_b)}\frac{\partial D_1(t_g, t_b)}{\partial t_b}\mathrm{d}t_b \\ &= \pi D_1^2(t_g, t_b)v_1(t_b)\,\mathrm{d}t_b. \end{aligned} \tag{25}$$

It must be considered that the growing grains touch with time. Therefore, only a fraction of the boundary $\Psi(f_1)$ will move, where $\Psi(f_1)$ is a function of the recrystallised volume fraction of the first recrystallisation cycle and $\Psi(f_1 = 1)$ has to be zero at the end of this cycle. Hence, the following relationship can be defined:

$$\psi(f) = 1 - \left(\frac{f - f_C}{1 - f_C}\right)^n S(f, f_C), \tag{26}$$

where f_C is the recrystallised volume fraction at the first contact time. The exponent n is an empirical constant factor and $S(f, f_C)$ is a switch function, whereat $f < f_C$: $S = 0$ and $f \geqslant f_C$: $S = 1$. With $\Psi(f_1)$, the volume increase in Eq. (25) becomes

$$\mathrm{d}V_1(t_g, t_b) = \Psi(f_1(t_b))\pi D_1^2(t_g, t_b)v_1(t_b)\,\mathrm{d}t_b \tag{27}$$

and so from Eqs. (21), (23) and (27) follows the volume of a grain at generation time t_g and observation time t_b

$$V_1(t_g, t_b) = \frac{\pi}{6}D_{cr1}^3(t_g) + \int_{t_g}^{t_b} \Psi(f_1(\tau))\pi D_1^2(t_g, \tau)v_1(\tau)\,\mathrm{d}\tau \tag{28}$$

and inserting Eq. (28) in Eq. (24) gives the total volume fraction of the recrystallised grains at observation time t_b

$$\begin{aligned} f_1(t_b) = &\int_{t_g = t_{cr1}}^{t_b}\int_{\tau = t_g}^{t_b} \Psi(f_1(\tau))\pi D_1^2(t_g, \tau)v_1(\tau)\,\mathrm{d}\tau\, R_{N1}(t_g) \\ &\times (1 - f_1(t_g))\,\mathrm{d}t_g + \frac{\pi}{6}\int_{t_g = t_{cr1}}^{t_b} D_{cr1}^3(t_g)R_{N1}(t_g) \\ &\times (1 - f_1(t_g))\,\mathrm{d}t_g \end{aligned} \tag{29}$$

with D_1 according to Eq. (21).

In Fig. 10, calculated DRX kinetics for a constant strain rate of $0.1\ \mathrm{s}^{-1}$ and a temperature of 1120 °C is compared

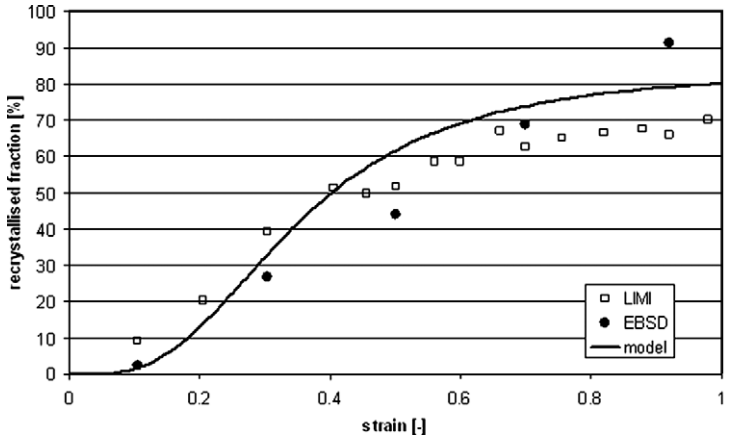

Fig. 10. Dynamic recrystallisation of Alloy 80A at a strain rate of 0.1 s^{-1} and a temperature of 1120 °C. Comparison of calculation (this model) and experiments [17].

with measured data. At a strain of 0.92, DRX has nearly completed (EBSD data, see also Fig. 19(e)). The LIMI data diverge from the EBSD data because the LIMI criterion used to distinguish between recrystallised and unrecrystallised grains seems to be unemployable for DRX fractions higher than about 70%. The calculated DRX fractions lie between the EBSD and the LIMI measurements.

6. Recrystallised grain size and grain size distribution

Assuming spherical grains, the mean size of recrystallised grains at a time of observation $D_{m1}(t_b)$ can be derived from the relationship between the mean volume of the recrystallised grains, the recrystallised fraction and the nuclei density

$$V_{m1}(t_b) = \frac{f_1(t_b)}{N_1(t_b)} = \frac{\pi D_{m1}^3(t_b)}{6} \tag{30}$$

with $N_1(t_b)$ according to Eq. (20).

Fig. 11 depicts the development of the mean recrystallised grain size with strain for calculated as well as for measured data. This size of the recrystallised grains does not change very much with strain, both for measured and calculated results. However, the LIMI data are ca. 20% lower than the EBSD data. In Fig. 11, the calculated size decreases somewhat with ongoing recrystallisation. This is because the nucleation rate decreases with continued recrystallisation (Eq. (20)) and the remaining deformed grain area is filled up with nuclei of critical size in the model, thus the mean DRX size lessens. In Fig. 12, DRX grain size of Alloy 80A is shown as a function of temperature and strain rate. As expected, the grain size increases with increasing temperature and decreasing strain rate.

There is a formation of dN_1 nuclei within the time period dt_g

$$dN_1(t_g) = R_{N1}(t_g)(1 - f_1(t_g))\, dt_g. \tag{31}$$

The relative number of the grains with a diameter between D_1 and $D_1 + dD_1$ is $g(D_1)\, dD_1$, if $g(D_1)$ is the function of the grain size distribution. Hence, $g(D_1)\, dD_1$ is equal to

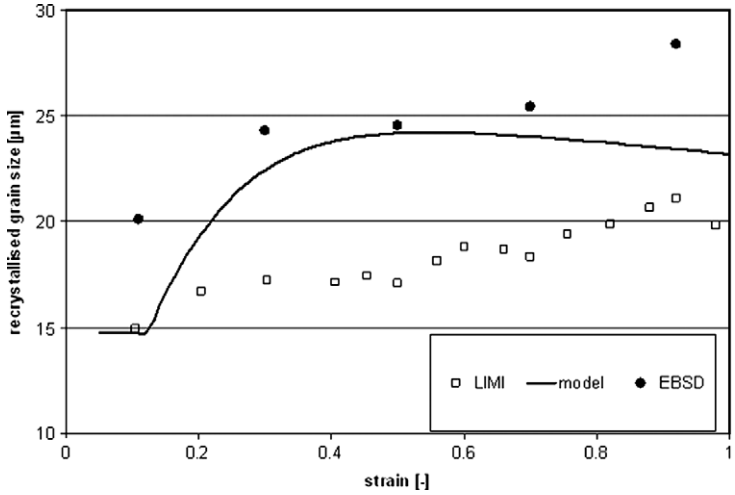

Fig. 11. Development of the mean DRX grain size with time (Alloy 80A, $T = 1120$ °C, $\dot{\varepsilon} = 0.1\ s^{-1}$). In both the EBSD and LIMI analysis, twins were removed (EBSD) and not etched (LIMI), respectively, to get comparable grain sizes [15,16].

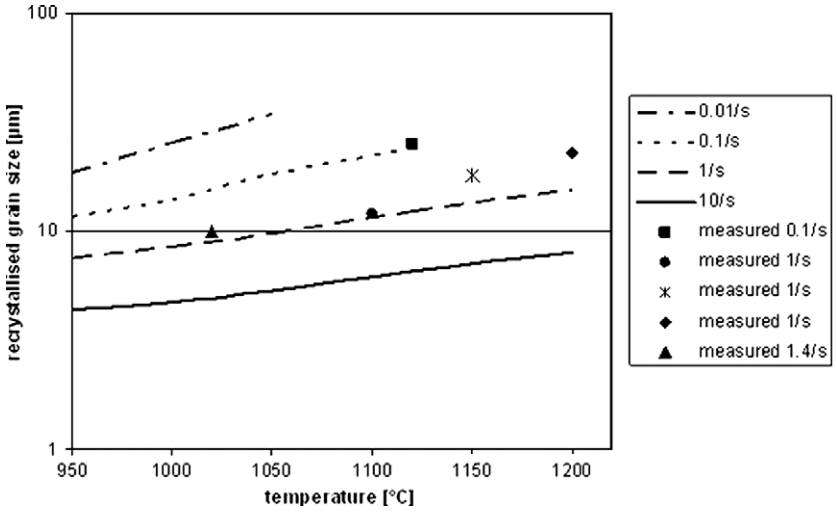

Fig. 12. Mean recrystallised grain size of Alloy 80A at different strain rates and temperatures. Comparison of calculations (this model) and experiments [30].

the relative number of grains which form between t_g and $t_g + dt_g$

$$\frac{dN_1(t_g)}{N_1(t_b)} = \frac{R_{N1}(t_g)}{N_1(t_b)}(1 - f_1(t_g))\,dt_g = g(D_1)\,dD_1, \tag{32a}$$

$$\frac{\partial D_1}{\partial t_g} = 2v_1(t_g) + \frac{dD_{cr1}(t_g)}{dt_g}, \tag{32b}$$

with $D_1 = D_1(t_g, t_b)$ according to Eq. (21). From Eqs. (32a) and (32b) follows the distribution function:

$$g(D_1(t_g, t_b)) = \frac{R_{N1}(t_g)(1 - f_1(t_g))}{N_1(t_b)\left[2v_1(t_g) + \frac{dD_{cr1}(t_g)}{dt_g}\right]}. \tag{32c}$$

The time of observation equals the time of deformation end t_e during experiments, therefore $t_b = t_e$. Since at the time of observation $t_b = t_e$ the time of generation t_g of a grain size class with size between D_1 and $D_1 + dD_1$ is not known, t_g must be eliminated from Eq. (32c). Thereto Eq. (21) has to be solved after t_g and the latter has to be inserted into Eq. (32c). This would result in an analytic expression of g as a function of D_1 with t_b as a parameter. Since this is not possible here, for a given D_1, $g(D_1)$ has to be determined numerically. Therefore t_g is iteratively calculated from Eq. (21) for several D_1 within the time interval $[t_{cr}, t_b]$ and used in Eq. (32c). Hence, values of the distribution function assigned to D_1 result. Using this function, the mean diameter within the recrystallised region is

$$D_{m1}(t_b) = \int_{D_{min}(t_b)}^{D_{max}(t_g)} D_1(t_g, t_b) g(D_1(t_g, t_b))\,dD_1. \tag{32d}$$

This definition of D_{m1} is equivalent to D_{m1} of Eq. (30).

Fig. 13 compares calculated and measured logarithmic size distributions of recrystallised grains for the Alloy 80A at a strain of 0.5 [16]. In the analysed EBSD data,

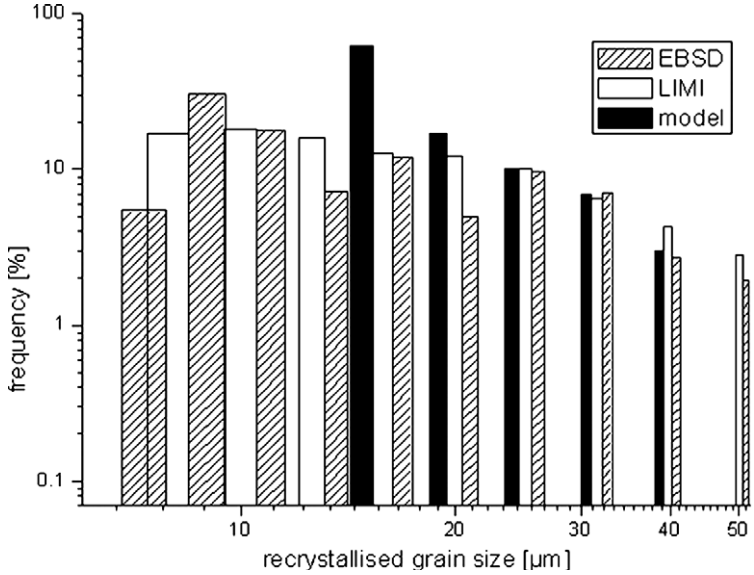

Fig. 13. Distribution of the mean recrystallised grain size (Alloy 80A, $T = 1120$ °C, $\dot{\varepsilon} = 0.1\ s^{-1}$, $\varepsilon = 0.5$) [15,16].

twins were removed to get comparable grain sizes [15]. The two-dimensional measured size distribution was transformed into a three-dimensional logarithmic distribution [31] to ensure comparability. The measured critical nucleus size seems to be around 6–10 μm (10.3 μm in the calculation) for these conditions. The maximum frequency of the measured data is situated at slightly lower values in comparison to the calculated data.

7. Dislocation density

The mean dislocation density ρ_1 within a recrystallised grain of diameter D_1 can be obtained by the quotient of the total dislocation length within the grain and the volume of the grains

$$\rho_1(t_b) = \frac{1}{V_1(t_b)}\left[\int_{t=t_g}^{t_b} \rho(\dot{\varepsilon}, t_b - t)\dot{V}_1(t)\,dt + \rho(\dot{\varepsilon}, t_b - t_g)\frac{\pi D_{cr1}^3}{6}\right]. \quad (33)$$

$V_1(t_b)$ and $\dot{V}_1(t)$ are given by Eqs. (28) and (25), furthermore ρ is calculated by Eq. (3b).

In Fig. 14, the maximum dislocation density at an arbitrary time of observation is in the centre of a recrystallised grain (i.e., within the critical radius). The local age and thus the local straining within this grain decreases with the distance to the centre. This should be valid at least in the early stages of a recrystallised grain, when the growing grains have not already touched. Summing up over all grain classes gives the mean dislocation density fraction $\rho_{m1}(t_b)$ within the region of the recrystallised grains

$$\rho_{m1}(t_b) = \frac{1}{f_1(t_b)}\left[\int_{t_g=t_{cr1}}^{t_b}\int_{\tau=t_g}^{t_b} \Psi(f_1(\tau))\pi D_1^2(t_g,\tau)v_1(\tau) \times \rho_1(\dot{\varepsilon}, t_b - \tau)\,d\tau\, R_{N1}(t_g)(1 - f_1(t_g))\,dt_g + \frac{\pi}{6}\int_{t_g=t_{cr1}}^{t_b} \rho_1(\dot{\varepsilon}, t_b - t_g)D_{cr1}^3(t_g)R_{N1}(t_g)(1 - f_1(t_g))\right]. \quad (34)$$

The dislocation length within the recrystallised volume fraction $f_1(t_b)$ is calculated by the sum of the integrals on the right hand side of this equation. Therefore, the expression in brackets has to be related to $f_1(t_b)$.

The total mean dislocation density during DRX can therefore be defined by

$$\rho_m(t_b) = \rho_0(t_b)(1 - f_1(t_b)) + \rho_{m1}(t_b)f_1(t_b) \quad (35)$$

where ρ_0 is the dislocation density of the unrecrystallised fraction (related to Eq. 3).

The modelled increase of the dislocation density from the moving grain boundary towards the grain centre (Fig. 14(b)) should have no main influence on the nucleation site. With grain boundary nucleation, the recrystallised grains do not grow very much further (Fig. 11, [33]). Hence, the dislocation density gradient cannot be very pronounced in the single DRX grains. This can also be deduced from Fig. 3, where the DRX grains seem to be rather equiaxed and of the same size. Also the grain orientation spread for the DRX grains shows a single and small peak in Fig. 3(a), thus indicating a rather even energy distribution over all DRX grains.

8. Second recrystallisation cycle

It is assumed that the nuclei of a second recrystallisation cycle will form at the contact points of the grains of the first cycle if the mean dislocation density of the first cycle reaches the critical dislocation density for the onset of dynamic recrystallisation. Both the critical dislocation density and the critical radius for the second recrystallisation cycle depend on the actual process conditions, i.e. strain rate and temperature that predicts the grain boundary and dislocation mobility, as well as the stationary dislocation density for dynamic recovery (Eq. 3). The nucleation rate within this second cycle changes with the size of the recrystallised grains of the first cycle D_{m1}. In the case of high recrystallisation rates compared to the strain rate, the second recrys-

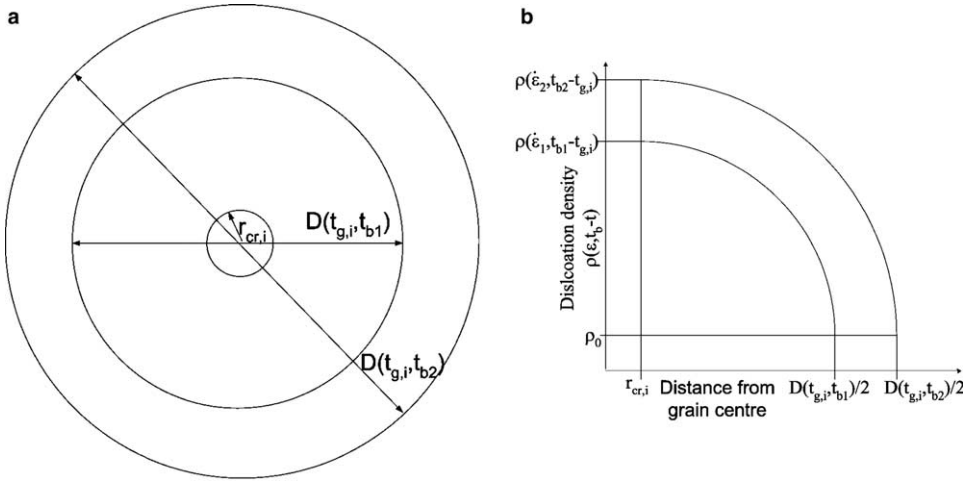

Fig. 14. Dislocation density within a recrystallising grain at times t_{b1} and t_{b2} (schematic depiction); grain size at times t_{b1} and t_2 (a); dislocation density distribution within grains at times t_{b1} and t_{b2} (b) [32]. The dislocation density decreases from the centre to the grain boundary. The level of the dislocation density increases with increasing strain ($\varepsilon_2 > \varepsilon_1$, i.e. time of observation $t_{b2} > t_{b1}$).

tallisation cycle will start before the first cycle has completed [34].

Up to now, only the first recrystallisation cycle was considered, which ends with $f = f_1 = 1$ and is not influenced by a second cycle. In the following, the indices $1, 2, \ldots, n$ represent the observed recrystallisation cycles. In analogy to Eq. (20), the number of nuclei of a second recrystallisation cycle that are formed within the first recrystallised fraction is

$$N_2(t) = \int_{t_{cr2}}^{t_b} R_{N_2}(t)(1 - f_2(t))\,dt = \int_{t_{cr2}}^{t_b} \frac{K_F R_{F2}(t)}{N_{d2} D_{m1}}(1 - f_2(t))\,dt, \quad (36)$$

where D_{m1} is the mean grain diameter of the first recrystallisation cycle, R_{N_2} is the nucleation rate per volume of the second recrystallisation cycle, $N_{d2} = A_{cr2}/l_{cr2}^2$ is the number of dislocations per critical nucleus, A_{cr2} is the cross-section of a critical nucleus and l_{cr2} is the mean free path of dislocations with a critical density ($l_{cr2} \sim \rho_{cr2}^{-1/2}$). The newly formed nuclei within the time step dt_g at the time t_g are

$$dN_2(t_g) = R_{N_2}(t_g)(1 - f_2(t_g))\,dt_g \quad (37)$$

thus the grain size distribution function $g_2(D_2)$ of the second recrystallisation cycle is defined by

$$\frac{dN_2(t_g)}{N_2(t_b)} = g_2(D_2)\,dD_2 = \frac{R_{N_2}(t_g)}{N_2(t_b)}(1 - f_2(t_g))\,dt_g, \quad (38)$$

which gives g_2 in analogy to Eq. (32c). Deducing from Eq. (29), the recrystallised fraction of the second generation is

$$f_2(t_b) = \int_{t_g=t_{cr2}}^{t_b} \int_{\tau=t_g}^{t_b} \Psi(f_2(\tau))\pi D_2^2(t_g,\tau) v_2(\tau)\,d\tau\, R_{N_2}(t_g) \times \left(1 - f_2(t_g)\right) dt_g + \frac{\pi}{6}\int_{t_g=t_{cr2}}^{t_b} D_{cr2}^3(t_g) R_{N_2}(t_g) \times (1 - f_2(t_g))\,dt_g, \quad (39)$$

where t_{cr2} is the time where the grains of the first recrystallisation cycle experience the critical conditions for the onset of a second recrystallisation cycle and v_2 is the grain boundary velocity of the second recrystallisation cycle in analogy to Eq. (22) ($\Delta\rho_2 = \rho_{m1} - \rho_{b2}(x = 0) \approx \rho_{m1}$), which can be calculated from the mean dislocation density of the first cycle ρ_{m1}

$$v_2 = m(\tau\Delta\rho_2 - P_Z)K_S. \quad (40)$$

In analogy to Eq. (34), the mean dislocation density fraction of the recrystallised grains of the second cycle is

$$\rho_{m2}(t_b) = \frac{1}{f_2(t_b)}\left[\int_{t_g=t_{cr2}}^{t_b}\int_{\tau=t_g}^{t_b} \Psi(f_2(\tau))\pi D_2^2(t_g,\tau) v_2(\tau) \times \rho_2(\dot{\varepsilon}, t_b - \tau)\,d\tau\, R_{N_2}(t_g)(1 - f_2(t_g))\,dt_g + \frac{\pi}{6}\int_{t_g=t_{cr2}}^{t_b} \rho_2(\dot{\varepsilon}, t_b - t_g) D_{cr2}^3(t_g) R_{N_2}(t_g)(1 - f_2(t_g))\,dt_g\right]. \quad (41)$$

9. Prediction of overall structure and flow stress

The total recrystallised volume fraction is assumed to be equal to the fraction of the first cycle ($f = f_1$) because the second recrystallisation front only exists within the recrystallised structure of the first generation. To describe the mean grain size D_m for all grain size classes and two recrystallisation cycles, a simple approach, shown here for two cycles, was chosen

$$D_m(t_b) = D_0(1 - f_1(t_b)) + D_{m1}(t_b)(f_1(t_b) - f_2(t_b)) + D_{m2}(t_b) f_2(t_b), \quad (42)$$

where the indices 1 and 2 denote the number of recrystallisation cycle, D_{m1} and D_{m2} are the mean grain size of the first and second recrystallisation cycle, respectively, and D_0 is the mean grain size of the unrecrystallised grains. Fig. 15 shows the calculated DRX and total mean grain sizes, as well as the recrystallised fractions with strain at a constant strain rate and temperature.

In Fig. 15, the mean grain size of the first cycle (D_{m1}) reaches a final size of 24 μm after a DRX fraction of ca. 30%. The second cycle (D_{m2}) starts at a strain of ≈0.68 and the corresponding recrystallised grains reach a final size of 18 μm.

In the case of two DRX cycles, for the calculation of the total mean dislocation density it has to be considered that all grains of the second generation lie within the first cycle structure. Hence, it follows in analogy to Eq. (42)

$$\rho_m(t_b) = \rho_0(t_b)(1 - f_1(t_b)) + \rho_{m1}(t_b)(f_1(t_b) - f_2(t_b)) + \rho_{m2}(t_b) f_2(t_b). \quad (43)$$

The second term in Eq. (43), $\rho_{m1}(f_1 - f_2)$, can be predicted by $\rho_{m1} f_1(1 - f_2/f_1)$, where $\rho_{m1} f_1$ is given with Eq. (34).

In Fig. 16, ρ_0 indicates the dislocation density in the unrecrystallised structure, which reaches a steady-state value after exceeding the critical value for recrystallisation. ρ_{m1} and ρ_{m2} are the mean dislocation densities of the first and second cycle, respectively. ρ_m denotes the total mean dislocation density, on which the flow curve is based. The grains of the second recrystallisation cycle reach the critical conditions for the onset of recrystallisation at a strain of ca. 0.85. Hence, a third recrystallisation cycle is initiated. The lack of the insertion of this third cycle into the model also leads to the not physically based rise of the total mean dislocation density at this critical strain.

The flow stress during hot forming in general depends on the resistance of the material to moving dislocations. At high temperatures, this resistance can be increased by sessile dislocations, particles and solute atoms, and not likely by grain boundaries

$$\sigma = M_T \alpha G b\sqrt{\rho_m} + \sigma_p + \sigma_s, \quad (44)$$

where M_T is the mean Taylor factor for poly-crystals, α is a constant, G is the shear modulus and σ_p and σ_s indicate the flow stress increase due to particles and solute atoms, respectively [32].

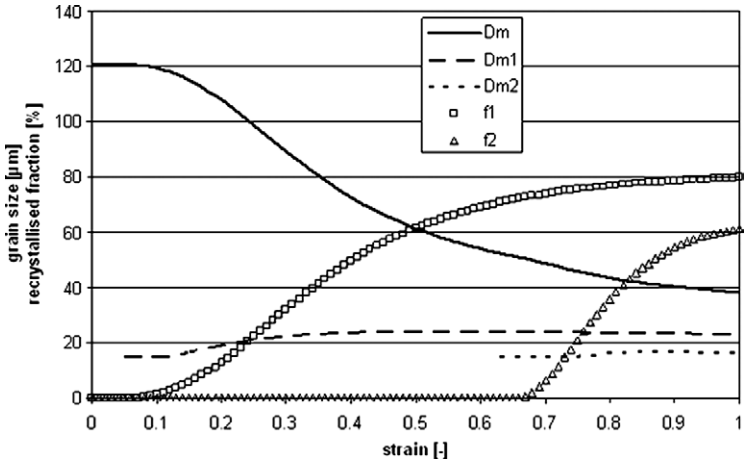

Fig. 15. Development of the calculated recrystallised mean grain size, as well as the recrystallised fraction within the first and second cycle and the total mean grain size during dynamic recrystallisation of Alloy 80A at $T = 1120$ °C and $\dot{\varepsilon} = 0.1\ s^{-1}$. The initial grain size is 120 μm.

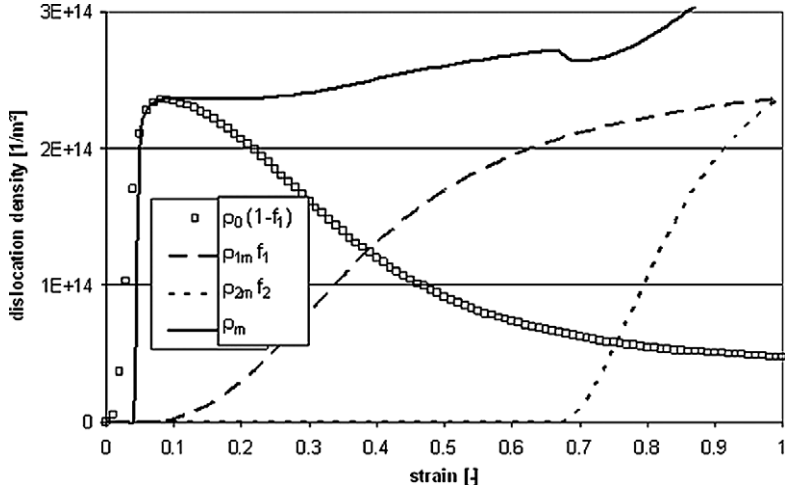

Fig. 16. Development of the calculated total mean dislocation density ρ_m and the dislocation density fractions of both the first $\rho_{1m}f_1$ and second $\rho_{2m}f_2$ recrystallisation cycle, as well as the unrecrystallised dislocation density fraction $\rho_0(1 - f_1)$ during dynamic recrystallisation of Alloy 80A at $T = 1120$ °C and $\dot{\varepsilon} = 0.1\ s^{-1}$. ρ_m does not correspond to the sum of the other dislocation density fractions because ρ_m is given by Eq. (43). Therefore, the kink of ρ_m is caused by the beginning of the second recrystallisation cycle. The initial grain size is 120 μm.

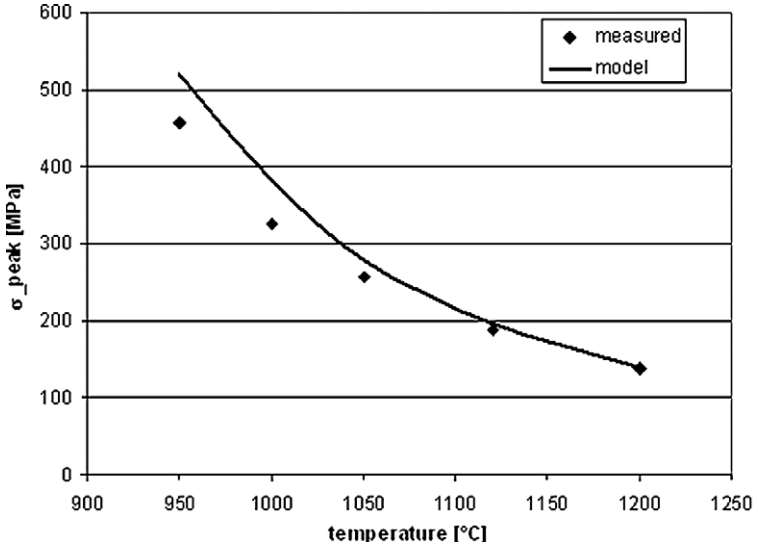

Fig. 17. Comparison of calculated and measured peak stresses from compression tests of Alloy 80A at $\dot{\varepsilon} = 1\ s^{-1}$.

In Fig. 17, measured and calculated peak stresses are compared for different temperatures at a constant strain rate of 1 s^{-1} (Alloy 80A).

10. Discussion

10.1. Conditions for dynamic recrystallisation

In Eq. (3) an approach of Stüwe [19,20], simplified by Sandström and Lagneborg [18] was chosen to describe the dislocation density rate during hot forming neglecting recrystallisation. In that work, only one overall class of dislocations was considered, neglecting the different densities in the subgrain walls and in-between. This might be an oversimplification because both the dislocation generation and the recovery rates are different for these regions. Recovery in the subboundaries was observed to be much slower than within the subgrains [18]. Next the size of the mean free path of dislocations in the subgrain interior may be quite large compared to that in the subgrain walls. With regard to recrystallisation, both types of dislocations contribute to the driving force. In [18], it is stated that the dislocation density in subgrain walls is so much greater than in the interior that the latter can be neglected from the point of view of DRX. Otherwise, it is proposed that the flow stress (Eq. (44)) is determined by the density of the interior dislocations. However, the volume ratio of the subgrain interior and the subgrain walls has to be considered.

However, in this work no attention was paid in the early development of the inhomogeneous distribution of the stored energy, i.e. the presence of subgrains. This is a serious omission at high Zener–Hollomon parameters (Z) when the critical nucleus size and the mean subgrain diameter become comparable. Also the theory predicts that DRX should not occur at high temperatures and low strain rates because the critical dislocation density is greater than that corresponding to a balance between work hardening and recovery. Such a deduction is not in accordance with e.g., DRX in creep. Hence, a proper consideration of the inhomogeneity of driving force distribution seems to be inevitable to account for the experimentally observed DRX behaviour over the whole range of Z.

10.2. Nucleation

Sakai and Ohashi [35] described the sub-structural evolution during the deformation of nickel. They showed that a cellular dislocation substructure developed even at very low strains. The cell size decreased and the cell boundaries became more clearly delineated with increasing strain until around the peak strain. The cell size and the dislocation density near the grain boundaries were, respectively, smaller and higher than those in the interior of the grain. Recrystallisation nuclei formed at the peak strain in the regions of greatest strain concentration, such as the existing grain boundaries. The dislocation sub-structures could be classified in three categories: DRX nuclei, containing very few dislocations; growing DRX grains, containing poorly developed sub-structures and a dislocation density gradient; large grains which contain fairly homogeneous and more clearly developed dislocation sub-structures. Both the DRX grain size at high strains and the cell size in the fully developed sub-structures increased systematically with decreasing Z (or flow stress) in nickel [36]. Thence the following correlations have been found: $d_c \sim D_{m1}^{0.77}$ and $\sigma_{peak} \sim D_{m1}^{-0.77}$.

There is strong evidence that DRX nuclei form by growth from pre-existing cells or subgrains in the deformed material [26]. The most likely method of forming a nucleus is by discontinuous growth of subgrains in orientation gradients. Faster growing subgrains acquire more misorientation and more mobile dislocations, thus resulting in the creation of high angle boundary and a nucleus when sufficient growth has occurred to reach the critical nucleus size. In addition, twinning can occur in metals of lower stacking fault energy, and there is evidence that this often occurs in the early stages of recrystallisation and may create the required mobile high angle boundary needed for recrystallisation [37]. The origin of recrystallisation at pre-existing high angle boundaries is known to be a very important mechanism, occurring particularly at lower strains and after high temperature deformation. Sakai [38] pointed out that nucleation of a DRX grain at grain boundaries consists of the following processes: boundary corrugation accompanied by the evolution of sub-boundaries; partial grain boundary sliding, leading to the development of inhomogeneous local strains; bulging of parts of a serrated grain boundary accompanied by the evolution of dislocation sub-boundaries or twinning. For austenitic steels, Frommert et al. [39] indicated that at high temperatures (1373 K) and low strains, new grains are generated by bulging of pre-existing grain boundaries and by local instabilities of the sub-structure near the grain boundary. This is in good accordance with the investigations of Alloy 80A (Fig. 3(b)). At lower temperatures ($T < 1273$ K) nucleation of DRX originated at initial grain boundaries by the mechanism of sub-structure growth into an orientation gradient.

Both subgrain growth in orientation gradients and nucleation at pre-existing grain boundaries require dislocation recovery mechanisms [26]. Hence in this work, a simple approach was used for the nucleation, namely that the nucleation rate at high temperatures in fcc materials with low stacking fault energies is governed by the recovery rate, thus on the climb velocity of edge dislocations.

10.3. Nucleation strands and cycles

In this work it was assumed that all DRX nuclei form at pre-existing grain boundaries of the deformed grains and thereafter grow into the deformed matrix. During the second DRX cycle, the nuclei form at the boundaries of the recrystallised grains, which are strained due to the

concurrent deformation. However, this would lead to elongated grains, because the growth within the nucleation plane (i.e., grain boundary plane) is hindered due to other nuclei. Gottstein [40] argued that after the first strand of necklace grains is completed along the prior grain boundary, it is quite difficult for bulging to take place at the interface because of the very high boundary curvature of the fine grains in the first strand. Sakai [38] stated that grain boundary sliding is expected to take place predominantly in the fine grained necklace regions. This brings out a high dislocation density gradient in these new grain interiors accompanied by grain rotation. Then the new grains in the second strand are expected to form by the bulging of portions of the interface between the first necklace region and the deformed matrix. Therefore, a more precise nucleation model should also include the formation of different strands within one recrystallisation cycle. Roberts et al. [41] made such an attempt to adapt Cahn's treatment of kinetics of grain boundary nucleated reactions [42] to dynamic recrystallisation in a model of repeated nucleation at the transformation interface.

The second DRX cycle most likely will start at the boundaries of the first strand of the DRX grains of the first cycle, which consist of the oldest and thus most strained grains of the first DRX cycle. If the latter experience a critical dislocation density, nuclei of the second DRX cycle will form here. That should be observable in the case of relatively large initial grains (i.e., few nucleation sites) and steady-state conditions with a small DRX grain size. Hence, the DRX grain size of the first cycle should be in between the size distributions of the initial and the DRX grains of the second DRX cycle. Fig. 18 depicts the grain size distribution measured by EBSD at a deformation state where a second DRX cycle should have been initiated and thus two grain size distributions should be observable if the assumptions from above are met (compare with Fig. 19(e)). There are not two explicit separated size distributions, but one could possibly distinguish between a first cycle and a second cycle with maximum frequencies at 24–32 and 6–12 μm, respectively. However, additional more precise investigations are necessary, particularly with differing initial grain sizes.

Multi-peak DRX (i.e., synchronised DRX) takes place at low Zener–Hollomon parameters and is characterised by the nucleation of all new grains between ε_{cr} and ε_{p} and the growth of these grains is restricted to the DRX interval within one cycle [43]. No further nucleation events occur during one DRX interval and growth is substantially before recrystallisation can once more be initiated; hence no necklaces can be found in this case. Here, the implemented nucleation model is restricted to continuous nucleation (see Section 4), i.e. the formation of a typical structure with DRX strands and thus cannot describe multi-peak DRX. However, in this paper, attention is turned on the DRX kinetic after nucleation. Thus the critical conditions for the onset of DRX as well as the nucleation rate are more or less input parameters for the developed model.

In the model presented, a second DRX cycle is initiated if the mean dislocation density of the first DRX grains exceeds the critical dislocation density. Thus the nucleation rate of the second cycle is related to the mean DRX grain size and the dislocation density of the first DRX cycle. The formulation of a third DRX cycle has not yet been implemented into the model, hence the calculated evolution of DRX is restricted to two cycles. A steady-state of DRX is fairly well reached within these two DRX cycles for the chosen example (Alloy 80A at $T = 1120\ ^{\circ}C$ and $\dot{\varepsilon} = 0.1\ s^{-1}$) thus two DRX cycles satisfy the representation of steady-state. Depending on the material, temperature and strain rate, steady-state could also be reached within a third or higher DRX cycle. In this case, the model would only describe a transient state of DRX.

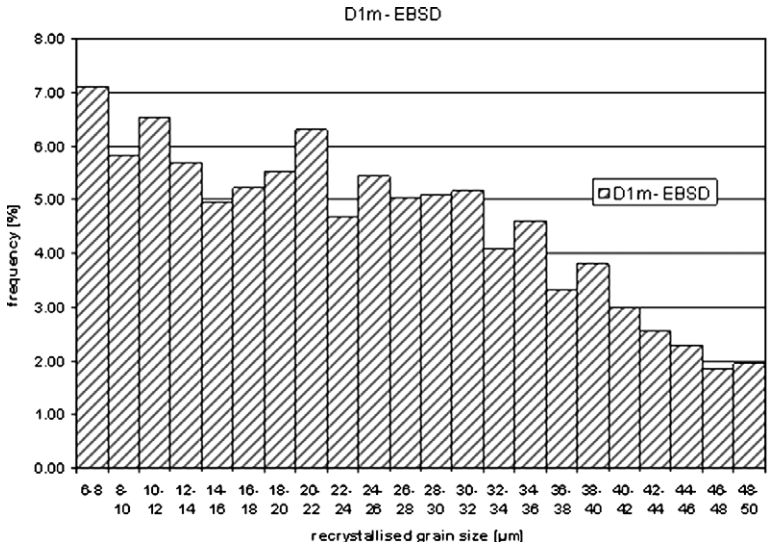

Fig. 18. Distribution of the recrystallised grain size (Alloy 80A, $T = 1120\ ^{\circ}C$, $\dot{\varepsilon} = 0.1\ s^{-1}$, $\varepsilon = 0.92$) [15].

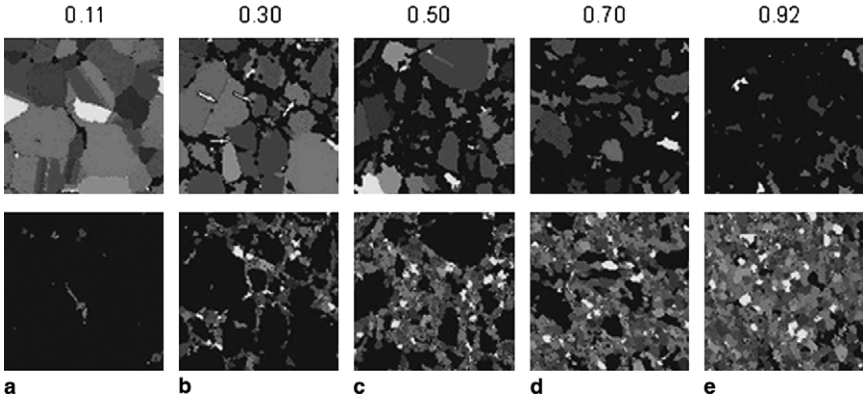

Fig. 19. Grain maps of both the deformed (top) and recrystallised (bottom) fraction as a function of strain, with the strain values atop of the image (coherent twins removed). The black areas represent the complementary fraction, the arrows show incoherent twins (0.30) [15].

10.4. Grain size development and recrystallisation rate

Concurrent deformation causes work hardening to take place within the dynamically growing grains, so that the driving force for growth is gradually reduced, becoming ineffective when the grains reach a stable size. The grain size during necklace recrystallisation can therefore be considered to be growth controlled (Eq. (21)). In the case of grain boundary nucleation, the DRX grain size immediately attains the final stable size [13]. This is because nucleation occurs essentially at the existing boundaries and the necklace mechanism generally operates. The measured data in Fig. 11 clearly indicate that not much further increase of the mean recrystallised grain size occurred after nucleation. In this model, there is no formation of different strands with equiaxed DRX grains considered, thus the recrystallised grains theoretically are able to grow further into the deformed grains. Indeed, if nucleation is confined exclusively to the pre-existing grain boundaries, then the resulting recrystallised grains should be elongated, which is in disagreement with experiments where dynamically recrystallised grains are observed to be equiaxed (Figs. 2 and 3(b)). In the presented theory, nucleation is considered as long there are unrecrystallised deformed grains left (Eq. (20)). Moreover, the recrystallisation behaviour can be tuned by a decreasing fraction of movable grain boundaries due to the contact between adjacent DRX grains (Eq. (29)). This is not really identical with the formation of DRX strands. However, with the two parameters f_c and n in Eq. (26), the recrystallisation rate can be adapted phenomenologically to experimental results. Fig. 19(d) indicates that at a strain of 0.70 (i.e., after a recrystallised fraction of ca. 70–80%, compare with Fig. 10), the formation of strands of recrystallised grains have nearly finished. There is only the innermost area of the deformed grains left which is confirmed by some few grains in Fig. 19(d) that were cut in their maximum cross-section and thus show some amount of unrecrystallised areas. With ongoing recrystallisation, the formation of DRX grains is finished and the remaining gaps between the small recrystallised grains are filled by the growth of the DRX grains (Fig. 19(e)). Hence, this retarded DRX rate is well represented by the decrease of the inclination of the calculated Avrami-type curve in Fig. 10.

11. Summary

In this work, a model for the description of dynamic recrystallisation is introduced. The total dislocation density is used as a state variable and predicts the onset of recrystallisation, if reaching critical conditions. The latter is deduced from maximising the net free energy based on the nucleation theory of spherical grains. It is shown that both the mobilities of dislocations and grain boundaries strongly affect the affinity of the material to initiate recrystallisation during hot deformation. The nucleation rate is calculated depending on the rate of generation of recovered dislocations that was found to depend on the climb velocity of edge dislocations for this type of alloys with relatively low stacking fault energies. The size of the recrystallising grains depends on the critical size of the recrystallisation nuclei, the nucleation rate and the velocity of the moving large angle grain boundaries. The recrystallised fraction can be derived from the number of recrystallised grains per volume and their mean volume. In each recrystallised grain, the dislocation density increases with time due to the ongoing deformation. If the dislocation density of the recrystallised grains reaches the corresponding critical strain for recrystallisation, a second recrystallisation cycle will start at the contact points of the recrystallised grains of the first cycle. With the help of both automatic image analysis systems and electron back scatter diffraction, calculated data can be compared to measurements. In the investigations, it was not possible to distinguish between recrystallised grains of a first and second recrystallisation cycle, respectively. Possibly, for better experimental investigations, very low strain rates are required to create conditions where a second recrystallisation cycle is initiated when the first cycle is nearly completed. However, such conditions also favour dynamic recovery instead of recrystallisation.

The model presented will be further developed by including a more precise description of the inhomogeneous distribution of deformation energy, i.e. subgrains and different dislocation classes. More emphasis will be placed on a detailed model of the nucleation of DRX strands within DRX cycles. A treatment of meta-dynamic recrystallisation related to the model presented here will be published.

Appendix A

List of symbols and relevant not time-dependent values for Alloy 80A at a temperature of 1120 °C and a strain rate of 0.1 s^{-1}. The indices 1 and 2 of the first and second recrystallisation cycles are omitted in this list.

A_{cr}	cross-section of a critical nucleus (1.7E − 10 m^2)
b	Burgers vector (2.5E − 10 m)
d_c	cell size in the fully developed sub-structure
D	grain size
D_{cr}	critical size of a recrystallisation nucleus (14.7E − 6 m)
D_m	total mean grain size
D_s	self-diffusivity (4E − 15 m^2/s)
D_0	mean grain size of unrecrystallised grains (120E − 6 m)
f	recrystallised fraction
f_c	recrystallised volume fraction at the first contact time of individual recrystallising grains
g	grain size distribution function
G	shear modulus (5.3E10 Pa)
ΔG	free energy change
K_F	constant (1.0)
K_S	solute drag for high boundaries velocities
l_{cr}	mean free path of dislocations with a critical density (1.2E − 8 m)
l_0	mean free path of dislocations within unrecrystallised grains
m	mobility of a high angle grain boundary (3.6E − 10 m^3/sN)
M	mobility of dislocations (1.0E − 5 m^2/sN)
M_T	Taylor factor for poly-crystals (3.06)
n	constant for the prediction of Ψ(0.5)
N	number of nuclei (i.e., grains) per volume
N_d	number of dislocations per critical nucleus (1.2E6)
N_p	number of potential nuclei per volume
P_N	probability for nucleation in case of $\varepsilon > \varepsilon_{cr}$
P_R	probability of recovery of dislocations (7.1E − 7)
P_Z	Zener drag
Q_{SD}	activation energy for self-diffusion (367.5 kJ/mol)
r	radius of a grain
r_{cr}	critical radius of a recrystallisation nucleus (7.35E − 6 m)
R_g	molar gas constant (8.3143 J/mol K)
R_F	rate of generation of recovered dislocations
R_N	nucleation rate per volume
S	switch function
t	time
t_b	time of observation
t_{cr1}	time of reaching the mean critical dislocation density of unrecrystallised grains (i.e., start of first recrystallisation cycle)
t_{cr2}	time of reaching the mean critical dislocation density of recrystallised grains of the first cycle (i.e., start of second recrystallisation cycle)
t_g	time of generation (i.e., nucleation time)
$t_{g,i}$	time of generation (i.e., nucleation time) of grain class i
x	local coordinate
V	grain volume
V_m	mean grain volume
α	constant
$\dot{\varepsilon}$	strain rate (0.1 s^{-1})
γ_{GB}	grain boundary energy per unit area (0.61 J/m^2)
ρ_b	increasing dislocation density in a new recrystallised grain behind the moving boundary
ρ_{cr}	critical dislocation density for the onset of dynamic recrystallisation (2.4E14 m^{-2})
ρ_s	stationary dislocation density for dynamic recovery (4.0E14 m^{-2})
ρ_m	total mean dislocation density
ρ_0	mean dislocation density of unrecrystallised grains
$\Delta\rho$	dislocation density difference at the recrystallisation front
σ	flow stress
σ_p	flow stress fraction due to particles
σ_{peak}	maximum flow stress
σ_s	flow stress fraction due to solute atoms
τ	average energy per unit length of dislocation (1.7E − 9 J/m)
Ψ	moveable fraction of a high angle grain boundary

References

[1] Buchmayr B, Auzinger D, Samoilov A, Sommitsch C. BHMMAM 2001;146:385.
[2] Sellars CM. Mater Sci Technol 1990;6:1072.
[3] Sommitsch C, Wieser V. Microstructural simulation of hot forming processes. In: Proceedings of the 7th European Conference on Advanced Materials and Processes, Associazione Italiana di Metallurgia, Rimini; 2001.
[4] Beynon J, Sellars CM. ISIJ Int 1992;32:359.
[5] Sommitsch C, Wieser V, Wurm C, Lenger H. BHMMAM 2001;146:6.
[6] Brand A, Karhausen K, Kopp R. Mater Sci Technol 1996;12:963.
[7] Buchmayr B, Samoilov A, Lachmann L, Aigmüller G. A fundamental TMCP rolling model for the prediction and optimisation of microstructure and properties of HSLA steels. In: Proceedings of the1st international conference on modelling of metal rolling processes. London: Imperial College; 1993. p. 134.
[8] Sommitsch D, Mitter W, Kleber S. Modelling recrystallization of nickel-base alloys. In: Proceedings of the international congress on advanced materials, their processes and applications. Munich: Werkstoffwoche-Partnerschaft; 2000.
[9] Sommitsch C, Wieser V, Kleber S. J Mater Proc Technol 2002;125–126:130.

[10] Luce R, Wolske M, Kopp R, Roters F, Gottstein G. Comput Mater Sci 2001;21:1.
[11] Sommitsch C, Kozeschnik E, Wasle G, Buchmayr B. A precipitation model for multi-phase systems in nickel-base superalloys. In: Chandra T, Higashi K, Suryanarayana C, Tome C, editors. Proceedings of the international conference on processing and manufacturing of advanced materials. Oxford: Elsevier; 2000.
[12] Srinivasan N, Prasad Y. Mater Sci Technol 1992;8:206.
[13] Sakai T, Jonas JJ. Acta Metall 1984;32:289.
[14] Roters F, Raabe D, Gottstein G. Acta Mater 2000;48:4181.
[15] Pölt P, Mitsche S, Sommitsch C, Walter M. EBSD – and the recrystallisation of Ni-base-alloys. In: Proceedings of the 13th European microscopy congress. Belgium: Belgian Society for Microscopy, University of Antwerp; 2004. p. 695.
[16] Walter M, Sommitsch C, Wedl F, Kleber S. Systematische Bestimmung des rekristallisierten Gefügeanteiles einer Nickelbasislegierung in Abhängigkeit vom Verformungsgrad. In: Portella P, editor. Forschritte in der metallographie. Frankfurt Main, Werkstoff-Informationsges; 2004. p. 245.
[17] Sommitsch C, Walter M, Wedl F, Wieser V. Mater Sci Forum 2003;426–432:743.
[18] Sandström R, Lagneborg R. Acta Metall 1975;23:387.
[19] Stüwe H-P. Acta Metall 1965;13:1337.
[20] Stüwe H-P, Ortner B. Met Sci 1974;8:161.
[21] Kocks UF, Mecking H. A mechanism for static and dynamic recovery. In: Haasen P, Gerold V, Kostorz G, editors. Proceedings of the international conference on strength of metals and alloys, vol. 1. Oxford: Pergamon Press; 1979. p. 345.
[22] Laasraoui A, Jonas JJ. Metall Trans A 1991;22:1545.
[23] Roberts W, Ahlblom B. Acta Metall 1978;26:801.
[24] Mayer R. personal communication; 2001.
[25] Derby B, Ashby M. Scripta Mater 1987;21:879.
[26] Humphreys F. Mater Sci Forum 2004;467–470:107.
[27] Wasle G, Sommitsch C, Kleber S, Buchmayr B, Clemens H. BHMMAM 2003;148:293.
[28] Zener C. TMS-AIME 1949;175:175.
[29] Cahn J. Acta Metall 1962;10:789.
[30] Bock G. Ermittlung von mikrostrukturellen Kennwerten bei der Warmformgebung von Nickelbasis-Superlegierungen. Diploma thesis, Graz University of Technology, Graz; 1998.
[31] Saltykov S. In: Stereometrische metallographie. Leipzig: VEB; 1974. p. 283.
[32] Sommitsch C. Theorie und Modell der mikrostrukturellen Entwicklung von nickel-basis-legierungen während des Warmwalzens – Die virtuelle Walzstraße. PhD thesis, Graz University of Technology, Graz; 1999.
[33] Sah J, Richardson G, Sellars C. Metall Sci 1974;8:325.
[34] Sakai T, Jonas JJ. Acta Metall 1984;32:189.
[35] Sakai T, Ohashi M. Mater Sci Technol 1990;6:1251.
[36] Ohashi M, Endo T, Sakai T, Jonas JJ. J Jpn Inst Met 1990;54:435.
[37] Humphreys F, Hatherly M. Recrystallization and related annealing phenomena. 2nd ed. Oxford: Elsevier; 2004.
[38] Sakai T. In: Yue S, Es-sadiqi E, editors. Thermomechanical processing of steel – Jonas JJ symposium. Canada: Canadian Institute of Mining, Metallurgy and Petroleum; 2000. p. 47.
[39] Frommert M, Brünger E, Wang X, Gottstein G. Mater Sci Forum 2004;467–470:937.
[40] Gottstein G, Brünger E, Ponge D. In: Jonas JJ, Bieter TR, Bowman KJ, editors. Advances in hot deformation, texture and microstructures. Warrendale, PA: The Metallurgical Society-AIME; 1994. p. 477.
[41] Roberts W, Boden H, Ahlblom B. Metall Sci 1979;03/04:195.
[42] Cahn J. Acta Metall 1956;4:449.
[43] Luton MJ, Sellars CM. Acta Metall 1969;17:1033.